IEEE Access
Multidisciplinary | Rapid Review | Open Access Journal

Received December 13, 2017, accepted January 13, 2018, date of publication January 18, 2018, date of current version March 16, 2018.

Digital Object Identifier 10.1109/ACCESS.2018.2794962

Microstrip Patch Antennas With Multiple Parasitic Patches and Shorting Vias for Bandwidth Enhancement

KAI DA XU[1,2,3], (Member, IEEE), HAN XU[1], YANHUI LIU[1], (Member, IEEE), JIANXING LI[4], AND QING HUO LIU[5], (Fellow, IEEE)

[1]Department of Electronic Science, Xiamen University, Xiamen 361005, China
[2]Shenzhen Research Institute of Xiamen University, Shenzhen 518057, China
[3]State Key Laboratory of Millimeter Waves, Southeast University, Nanjing 210096, China
[4]School of Electronic and Information Engineering, Xi'an Jiaotong University, Xi'an 710049, China
[5]Department of Electrical and Computer Engineering, Duke University, Durham, NC 27708, USA

Corresponding author: Yanhui Liu (yanhuiliu@xmu.edu.cn)

This work was supported in part by the National Natural Science Foundation of China under Grant 61601390, in part by the State Key Laboratory of Millimeter Waves Open Research Program under Grant K201813, and in part by the Guangdong Natural Science Foundation under Grant 2016A030310375, and in part by Science and Technology Research Project of Fujian Province under Grant 2017I0017.

ABSTRACT Two novel microstrip patch antennas with multiple parasitic patches and shorting vias have been presented for the bandwidth enhancement. Based on the conventional triangular patch antenna, two more resonances can be obtained with the introduction of multiple parasitic patches, and consequently, the antenna bandwidth can be broadened. Parametric analysis of the patches has been studied for the verification of bandwidth enhancement. An example of the proposed antenna with multiple parasitic patches is designed, fabricated, and tested. The measured bandwidth with $|S_{11}| < -10$ dB ranges from 5.46 to 6.27 GHz (13.8%), and good far-field radiation patterns can be obtained within the frequency band. In addition, two shorting vias are inserted into the above proposed antenna to decrease the input impedance, resulting in further bandwidth enhancement of the antenna. This antenna is fabricated and tested as well, which achieves a measured 10-dB impedance bandwidth of 17.4% from 5.5 to 6.55 GHz.

INDEX TERMS Bandwidth enhancement, microstrip patch antennas, parasitic patch, shorting vias.

I. INTRODUCTION

With the rapid growth of modern wireless communication systems, the demand for antennas with light weight and low profile has been increasing significantly. Due to the advantages of low profile, light weight and high gain, microstrip antennas are very attractive in many transceiver system applications [1]. However, conventional microstrip antennas suffer from narrow impedance bandwidths due to its single resonance radiation, typically less than 5% [2]. Therefore, several methods have been presented to enhance the bandwidth of the microstrip patch antennas [3]–[15]. One of the most popular ways is to introduce some slots into the patch radiators [3]–[5], which can yield extra controllable resonances for the bandwidth enhancement. This approach has the advantage of simple antenna structures without introducing additional sizes, however, the radiation patterns may be affected in some degree. Another widely used method is adding parasitic strips or patches for gap-coupling to the main patch radiators [6]–[9]. For instance, a microstrip antenna with gap-coupled sectoral patch has been designed in [6], which results in a bandwidth increase from 1.6% to 12.3%. In [9], a multilayer antenna structure is used for improving the impedance bandwidth. Although the multilayer dielectrics and patches can achieve an enhanced impedance bandwidth of over 20%, it pays a heavy price for the increased profile and cost. Additionally, inserting shorting vias into the dielectric substrate is one of the prevailing approaches used by researchers recently [10]–[15]. In [10], a triangular patch antenna using shorting vias and V-shaped slot is proposed, where a wider bandwidth is obtained with the help of the shorting vias, having great influence on the resistance and reactance of the antenna. Similarly, in [11]–[15] the shorting vias are inserted in order to expand the impedance bandwidths of the antennas.

In this paper, an equicrural triangular microstrip patch antenna with multiple parasitic patches around the main patch is presented. Three resonances can be obtained due to the introduction of the three parasitic patches. The effect of each parasitic patch has been explored sequentially and some key parameters have been analyzed. Seen from the measured results, the 10-dB impedance bandwidth of the designed antenna is 5.46∼6.27 GHz (13.8%). Then, two shorting vias are inserted based on the above designed antenna, consequently, an even wider impedance bandwidth can be yielded, from 5.5 to 6.55 GHz (17.4%). The measured return losses and radiation patterns of the proposed antenna agree well with the simulated ones.

II. DESIGN OF MICROSTRIP PATCH ANTENNA WITH MULTIPLE PARASITIC PATCHES

Fig. 1 illustrates the geometry evolution of the designed antennas and their simulated reflection coefficients. The antennas are printed on the top of an FR4 substrate with a relative permittivity of $\varepsilon_r = 4.4$ and a thickness of $h = 1.6$ mm, and the ground is printed on the bottom of substrate. Each antenna is fed by 50 Ohm coaxial probe through SMA connector. A full-wave electromagnetic simulator Ansys HFSS [16] is utilized to analyze the designed antennas. The antenna Ant_1 is shown in Fig. 1(a) with a simple equicrural triangular patch (D), whose simulated result is displayed in Fig. 1(d). As shown in Fig. 1(b), the antenna ANT_2 consists of the equicrural triangular patch (D) and a trapezoid parasitic patch (P1) on its right-handed side. Compared with the antenna ANT_1, the antenna ANT_2 has one more resonant mode introduced by P1, as presented in Fig. 1(d). To further broaden the antenna bandwidth, two right triangular parasitic patches (P2 and P2') are added based on the antenna ANT_2, as shown in Fig. 1(c). From Fig. 1(d) it is clear that the antenna ANT_3 has three resonances, resulting in a much wider bandwidth than those of antennas ANT_1 and ANT_2.

A. ANALYSIS OF THE ANTENNA ANT_1

The geometrical parameters of the antenna ANT_1 are illustrated in Fig. 1(a). It is composed of the simple equicrural triangular driven patch on the top of substrate and the ground plane beneath the substrate whose size is the same as that of the substrate. Fig. 1(d) shows the reflection coefficient of the antenna ANT_1, which has only one resonant mode.

For the antenna ANT_1, the resonant frequency of TM_{10} mode can be calculated by [17]

$$f_{TM_{10}} = \frac{2c}{3L_1\sqrt{\varepsilon_r}} \tag{1}$$

where c is the velocity of light in free space. It is indicated from (1) that the resonance of the antenna ANT_1 can be controlled by the parameter L_1. The simulation of the reflection coefficient versus L_1 is shown in Fig. 2. The resonant frequency will be shifted from 5.79 to 5.62 GHz when L_1 increases from 15.8 to 16.4 mm. It is clear that the resonant frequency decreases with the increase of L_1, which agrees with equation (1).

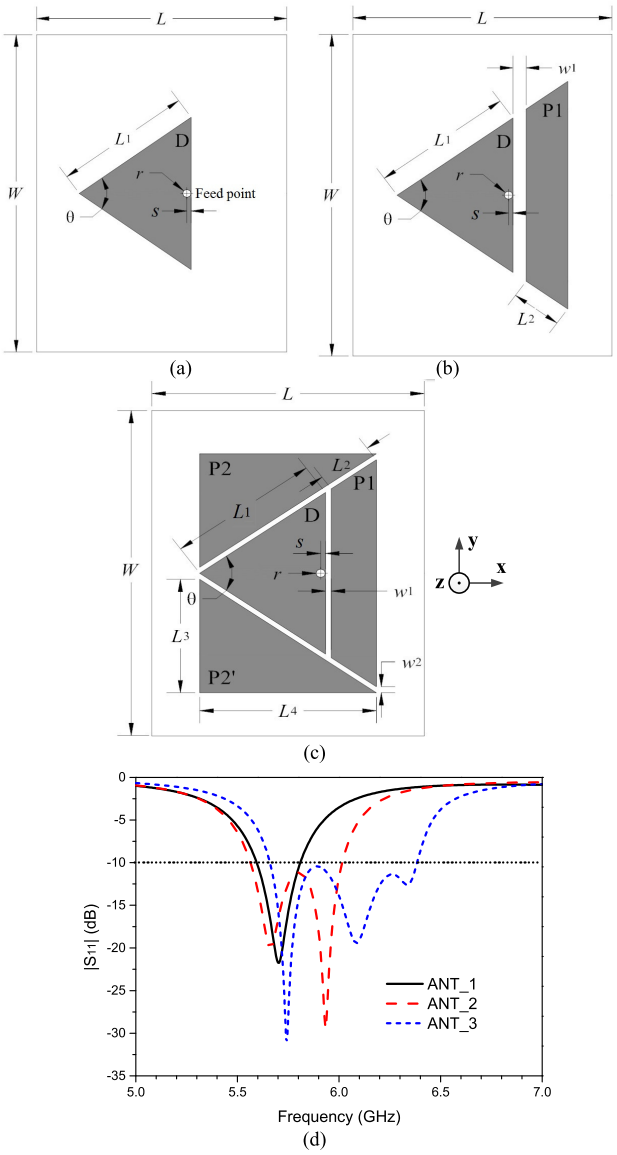

FIGURE 1. Geometry evolution of the designed antennas (a) ANT_1, (b) ANT_2, (c) ANT_3, and (d) their simulated reflection coefficients, where $L = 36$ mm, $W = 39$ mm, $L_1 = 16.1$ mm, $L_2 = 5.8$ mm, $w_1 = 1.5$ mm, $w_2 = 0.7$ mm, $s = 1$ mm, $\theta = 71°$ and $r = 0.65$ mm.

B. ANALYSIS OF THE ANTENNA ANT_2

In order to broaden the bandwidth, the antenna ANT_2 with a trapezoidal parasitic patch P1 closely coupled to the patch D is designed as shown in Fig. 1(b). Fig. 1(d) illustrates its reflection coefficient with two resonant modes, resulting in a wider bandwidth compared with that of the antenna ANT_1. It is obvious that one more resonance can be obtained when the extra parasitic patch P1 is added.

To analyze the effect brought by the patch P1, the surface current distribution of the antenna ANT_2 is studied, as shown in Fig. 3. At 5.66 GHz, the strong current

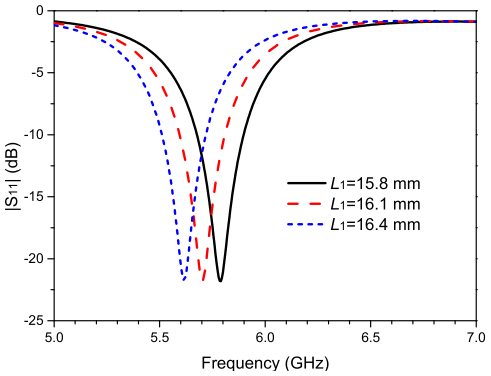

FIGURE 2. Simulated reflection coefficients of the antenna ANT_1 against L_1, where $\theta = 71$, $r = 0.65$ mm and $s = 1$ mm.

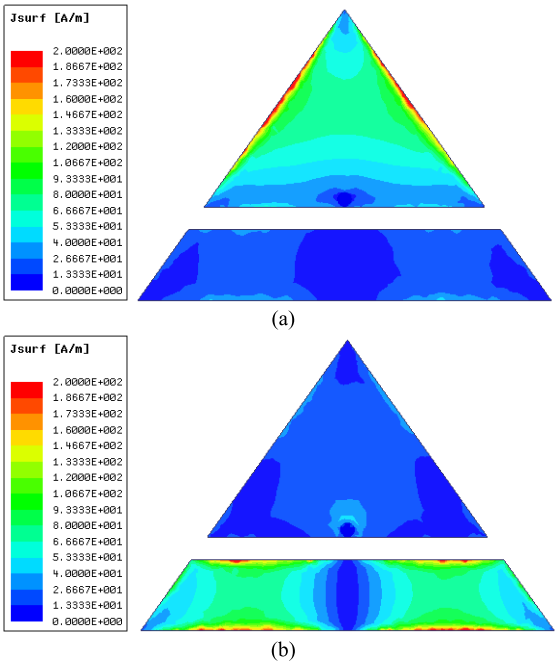

FIGURE 3. Surface current distribution of the antenna ANT_2 at (a) 5.66 GHz and (b) 5.92 GHz.

distribution mainly focuses on the equicrural triangular patch D as shown in Fig. 3(a), while in Fig. 3(b) the strong current magnitude is distributed on the trapezoidal patch P1 at 5.92 GHz. The first resonant mode of the antenna ANT_2 at 5.66 GHz is the TM_{10} mode, which has been analyzed in the Section II-A, but the second resonant mode at 5.92 GHz is the extra mode introduced by the trapezoidal patch P1. From Fig. 3(b), it can be found that the extra mode is the TM_{12} mode on the trapezoidal patch P1 where two periods of variation can be observed along the horizontal direction of trapezoid patch. To study the effect of parameters on this second resonant mode, the trapezoidal patch can be regarded as an annular patch for simplicity. Therefore, the resonant frequency of the TM_{12} mode can be calculated by [7]

$$f_{TM_{12}} = \frac{2c}{\theta(R_{ie} + R_{oe})\sqrt{\varepsilon_r}} \tag{2}$$

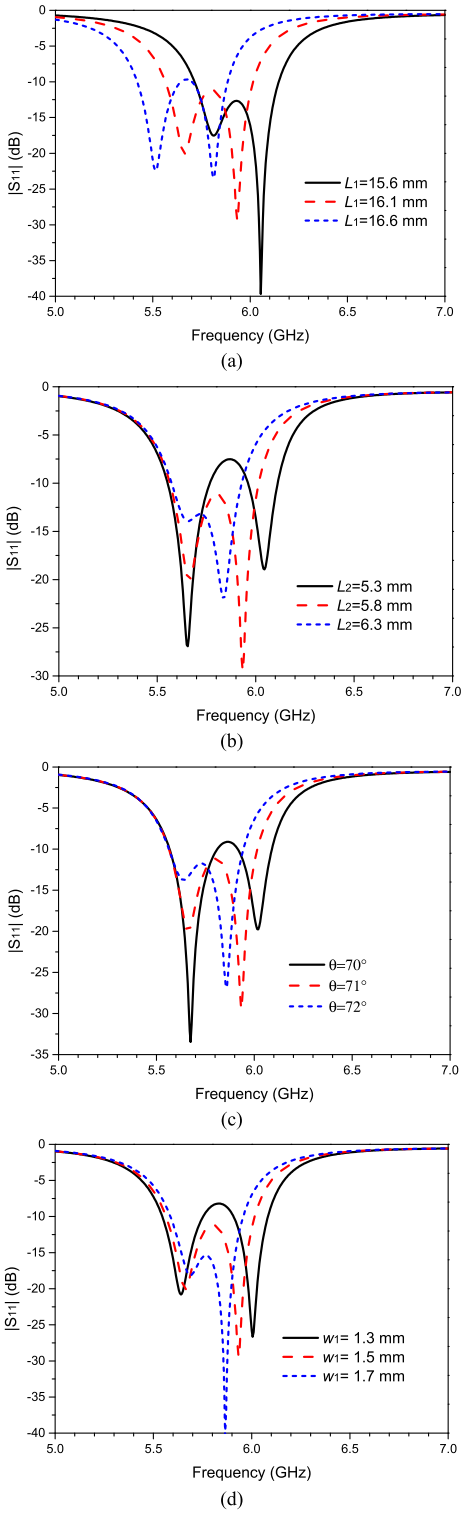

FIGURE 4. Simulated reflection coefficients of the antenna ANT_2 against (a) L_1, where $L_2 = 5.8$ mm, $\theta = 71°$, $w_1 = 1.5$ mm, $r = 0.65$ mm and $s = 1$ mm, (b) L_2, where $L_1 = 16.1$ mm, $\theta = 71°$, $w_1 = 1.5$ mm, $r = 0.65$ mm and $s = 1$ mm, (c) θ, where $L_1 = 16.1$ mm, $L_2 = 5.8$ mm, $w_1 = 1.5$ mm, $r = 0.65$ mm and $s = 1$ mm and (d) w_1, where $L_1 = 16.1$ mm, $L_2 = 5.8$ mm, $\theta = 71°$, $r = 0.65$ mm and $s = 1$ mm.

where R_{ie} and R_{oe} are the effective inner and outer radii of the annular patch, respectively. They can be obtained

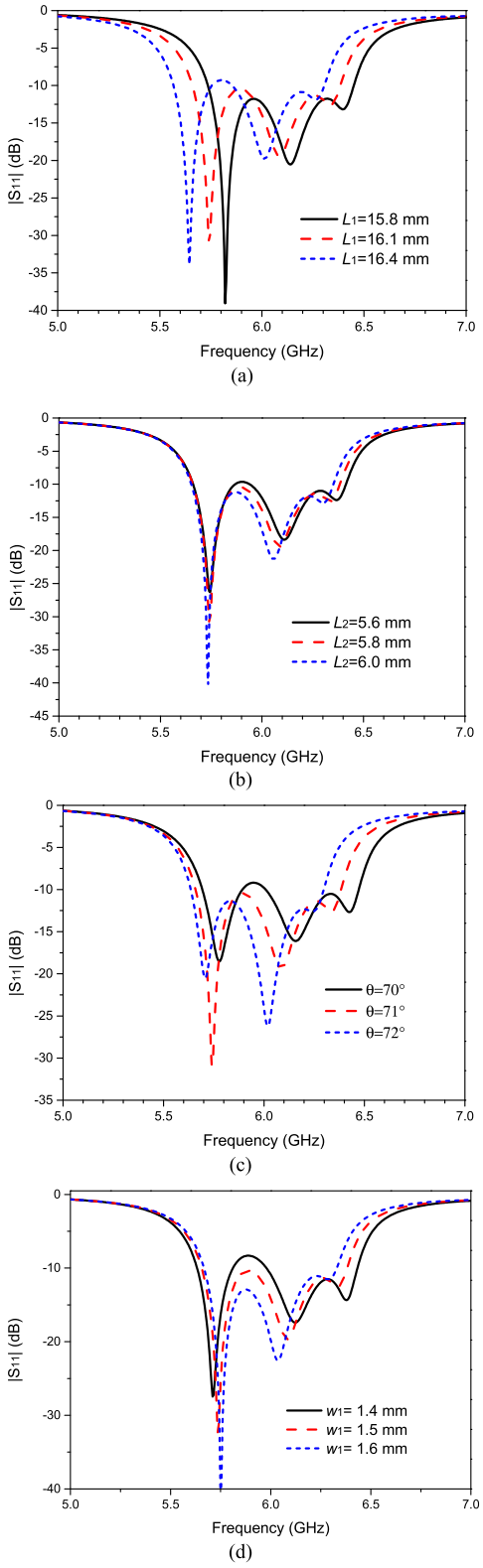

FIGURE 5. Simulated frequency responses of the antenna ANT_3 against (a) L_1, where $L_2 = 5.8$ mm, $\theta = 71°$, $w_1 = 1.5$ mm, $w_2 = 0.7$ mm, $r = 0.65$ mm and $s = 1$ mm, (b) L_2, where $L_1 = 16.1$ mm, $\theta = 71°$, $w_1 = 1.5$ mm, $w_2 = 0.7$ mm, $r = 0.65$ mm and $s = 1$ mm, (c) θ, where $L_1 = 16.1$ mm, $L_2 = 5.8$ mm, $w_1 = 1.5$ mm, $w_2 = 0.7$ mm, $r = 0.65$ mm and $s = 1$ mm, and (d) w_1, where $L_1 = 16.1$ mm, $L_2 = 5.8$ mm, $\theta = 71°$, $w_2 = 0.7$ mm, $r = 0.65$ mm and $s = 1$ mm.

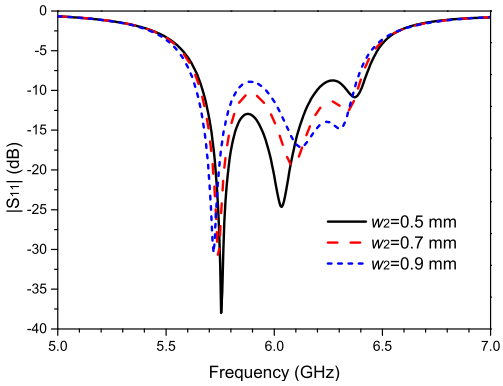

FIGURE 6. Simulated frequency responses of the antenna ANT_3 against w_2, where $L_1 = 16.1$ mm, $L_2 = 5.8$ mm, $\theta = 71°$, $w_1 = 1.5$ mm, $r = 0.65$ mm and $s = 1$ mm.

by

$$R_{ie} = R_i\sqrt{1 + \frac{2h}{\pi R_i \varepsilon_r}(\ln\frac{\pi R_i}{2h} + 1.7726)} \tag{3}$$

$$R_{oe} = R_o\sqrt{1 + \frac{2h}{\pi R_o \varepsilon_r}(\ln\frac{\pi R_o}{2h} + 1.7726)} \tag{4}$$

where R_i and R_o are the inner and outer radii of the annular patch, respectively. For the antenna ANT_2, these two parameters can be calculated approximately by

$$R_i \approx L_1\cos(\theta/2) + w_1 \tag{5}$$

$$R_o \approx (L_1 + L_2)\cos(\theta/2) + w_1 \tag{6}$$

From (2)-(6), it is indicated that the resonant frequency of the TM_{12} mode depends on the parameters of L_1, L_2, θ and w_1. The simulated reflection coefficients versus L_1, L_2, θ and w_1 are shown in Fig. 4. It can be observed from Fig. 4(a) that both of these two resonances are moved to the lower frequencies with the increase of L_1. However, as shown in Fig. 4(b)-(d), when L_2, θ or w_1 increases, the second resonant frequency decreases while the first one almost keeps constant. These results are in accordance with the equations (1)-(6), therefore, these parameters can be tuned to attain the required center frequency and impedance bandwidth of the antenna ANT_2.

C. ANALYSIS OF THE ANTENNA ANT_3

For further bandwidth enhancement, two right triangular parasitic patches P2 and P2' are positioned on two sides of the antenna ANT_2 to construct the antenna ANT_3, as shown in Fig. 1(c). Fig. 1(d) already showed the reflection coefficient of the antenna ANT_3 compared with those of the antennas ANT_1 and ANT_2. It can be found that three resonances can be obtained when the patches P2 and P2' are introduced, resulting in a wider impedance bandwidth, whereas the size of antenna is not increased.

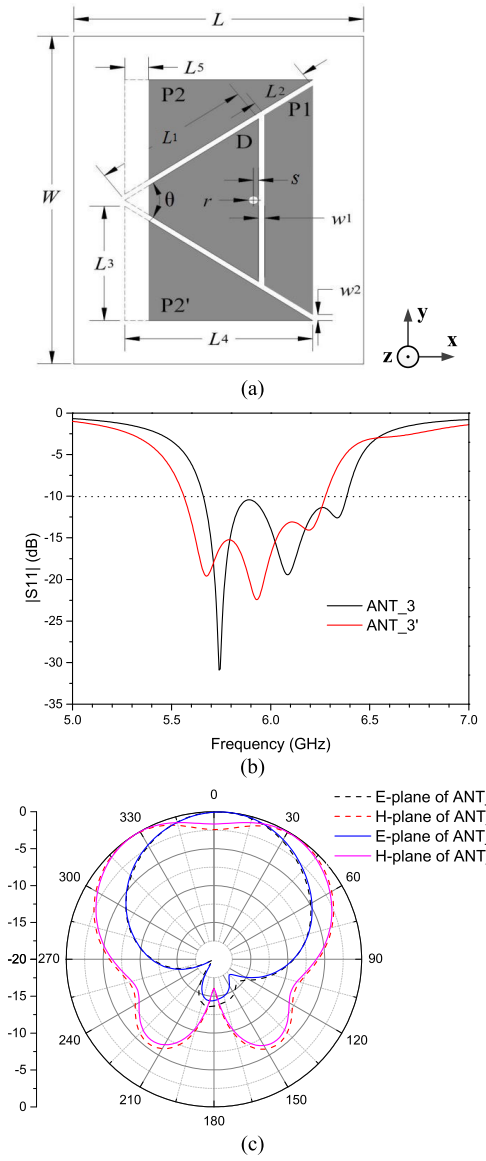

FIGURE 7. (a) Geometry of the antenna ANT_3′, and comparisons of (b) simulated reflection coefficients and (c) radiation patterns at 6 GHz between the antennas ANT_3 and ANT_3′.

For the right triangular patches P2 and P2', the parameters L_3 and L_4 can be calculated by

$$L_3 = ((L_1 + L_2)\cos\frac{\theta}{2} + w_1)\tan\frac{\theta}{2} \tag{7}$$

$$L_4 = (L_1 + L_2)\cos\frac{\theta}{2} + w_1 \tag{8}$$

Similarly to the deduction of Section II-A, the resonant frequency of the third resonant mode introduced by the patches P2 and P2' can be calculated by

$$f_{M3} = \frac{2c}{3\frac{L_3}{\sin(\theta/2)}\sqrt{\varepsilon_r}} = \frac{2c}{3(L_1 + L_2 + \frac{w_1}{\cos(\theta/2)})\sqrt{\varepsilon_r}} \tag{9}$$

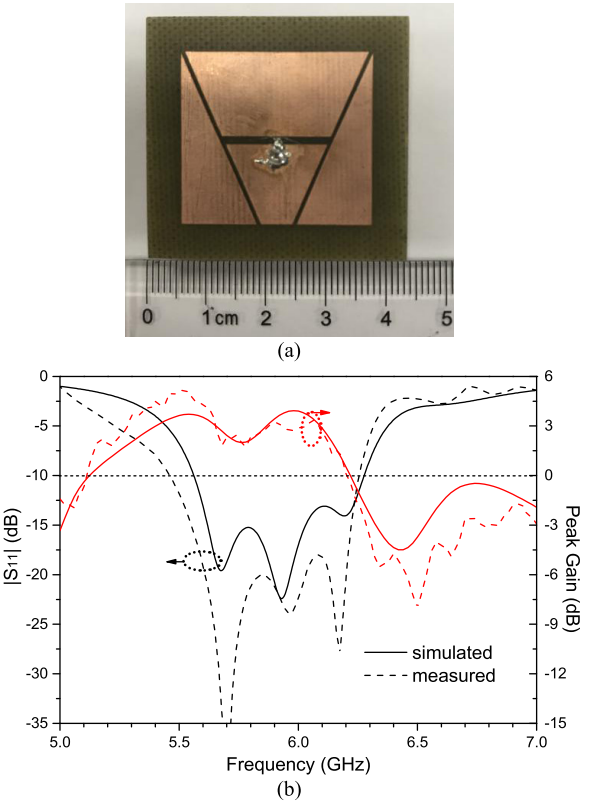

FIGURE 8. (a) Photograph and (b) simulated and measured reflection coefficients and peak gains of the proposed antenna ANT_3′.

or

$$f_{M3} = \frac{2c}{3\frac{L_4}{\cos(\theta/2)}\sqrt{\varepsilon_r}} = \frac{2c}{3(L_1 + L_2 + \frac{w_1}{\cos(\theta/2)})\sqrt{\varepsilon_r}} \tag{10}$$

Consequently, this resonant mode will be affected by the four parameters L_1, L_2, w_1 and θ. The simulated reflection coefficients of the antenna ANT_3 versus these four different parameters are illustrated in Fig. 5. As shown in Fig. 5(a), when L_1 increases from 15.8 to 16.4 mm, three resonant frequencies will all decrease, thus the center frequency of the antenna ANT_3 will shift from 6.10 to 5.94 GHz, while the bandwidth will keep almost unchanged. From Fig. 5(b)-(d), it can be observed that the second and third resonances will be both moved as the parameter L_2, θ or w_1 varies, while the first resonance almost remains the same, which are in accordance with the above-mentioned equations. It is noteworthy that the gap w_2 is also a key parameter which determines the coupling between the right rectangular patch (P2 or P2') and the other two patches (D and P1) of the ANT_3. The simulated frequency responses against different values of w_2 are plotted in Fig. 6. These above parameters should be properly tuned to eventually obtain a required broad impedance bandwidth.

In order to reduce the operating frequency of the antenna but not increase its size, the antenna geometry (i.e., ANT_3') is slightly modified as shown in Fig. 7(a), where the radiator patch D is cut into a trapezoidal patch and the right rectangular patches (P2 and P2') are also cut, meanwhile,

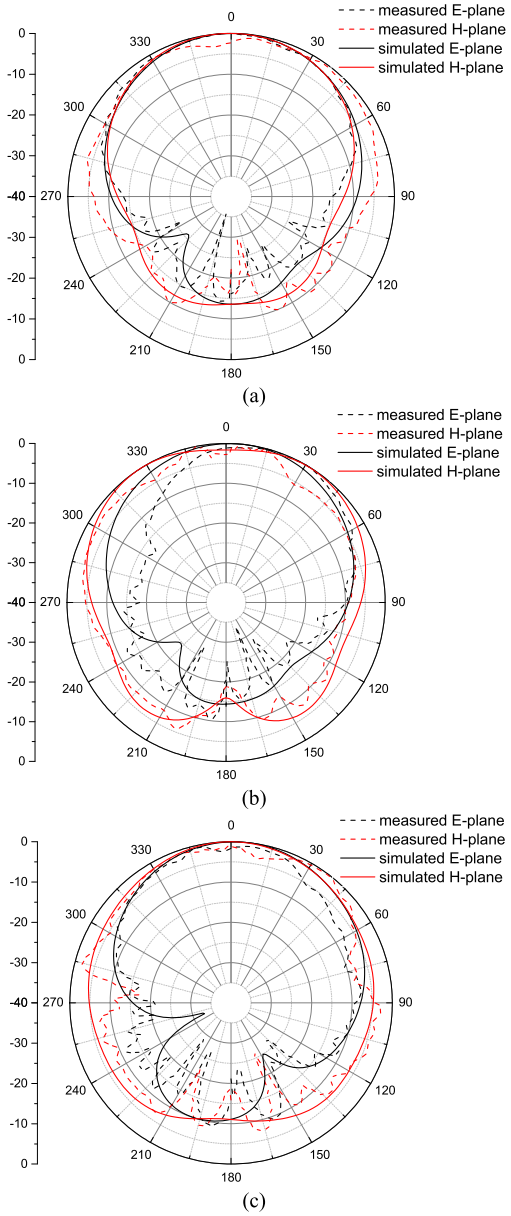

FIGURE 9. Simulated and measured radiation patterns at (a) 5.7 GHz, (b) 6.0 GHz and (c) 6.2 GHz.

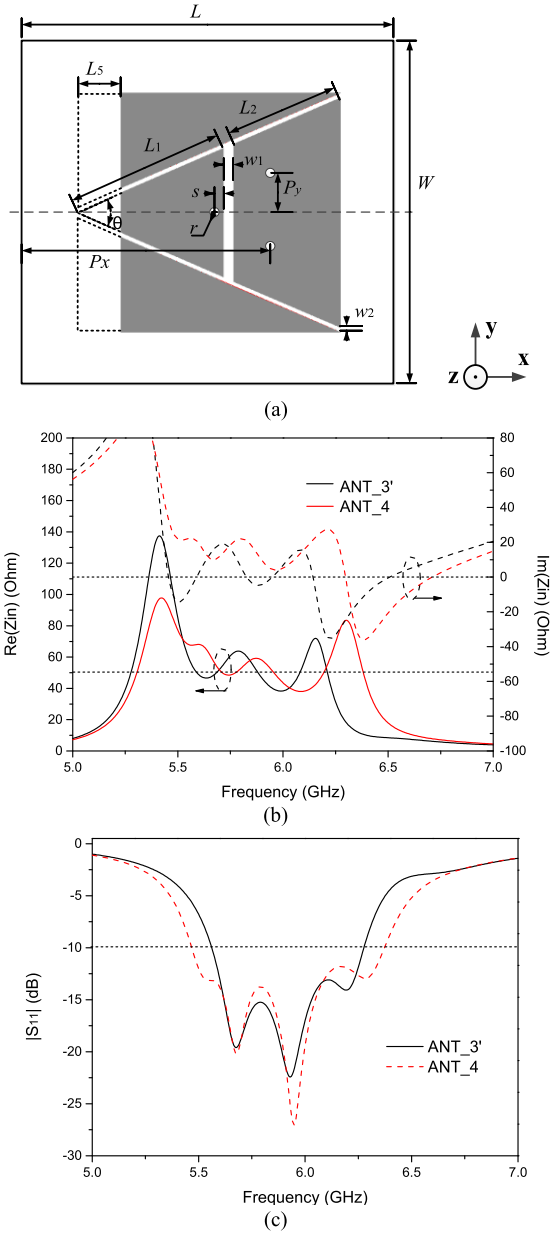

FIGURE 10. (a) Geometry of the antenna ANT_4, and comparisons of (b) input impedances and (c) reflection coefficients between the antennas ANT_4 and ANT_3'.

the parameter θ is decreased from 71° to 47°. In Fig. 7(b), it can be observed that the center frequency of the antenna ANT_3' is decreased but the absolute bandwidth almost remains the same compared with that of the antenna ANT_3. On the other hand, owing to the truncation of the patch D and the decrease of θ, the sizes of the patches P2 and P2' are effectively reduced, resulting in the influence reduction of the radiation patterns. The simulated radiation patterns of the antennas ANT_3 and ANT_3' at 6 GHz are shown in Fig. 7(c). It can be observed that the maximum realized gains in H-plane (yz-plane) are not toward the boresight direction (z-axis direction), which are caused by the parasitic patches P2 and P2'. At the boresight direction, the radiation pattern of ANT_3' in H-plane is improved compared with that of ANT_3. Nevertheless, three resonant modes of the antenna still exist and the center frequency can be reduced.

D. MEASUREMENTS OF THE ANTENNA ANT_3'

Based on the above analysis, the microstrip patch antenna ANT_3' with three resonances is designed and optimized. The final dimensions of the fabricated antenna ANT_3' are chosen as follows: $L = 36$ mm, $W = 39$ mm, $L_1 = 18.8$ mm, $L_2 = 13.5$ mm, $L_5 = 5.4$ mm, $w_1 = 1.2$ mm, $w_2 = 0.6$ mm, $s = 1.3$ mm, $\theta = 47°$ and the radius of the probe $r = 0.65$ mm. The driven patch D is fed by a coaxial

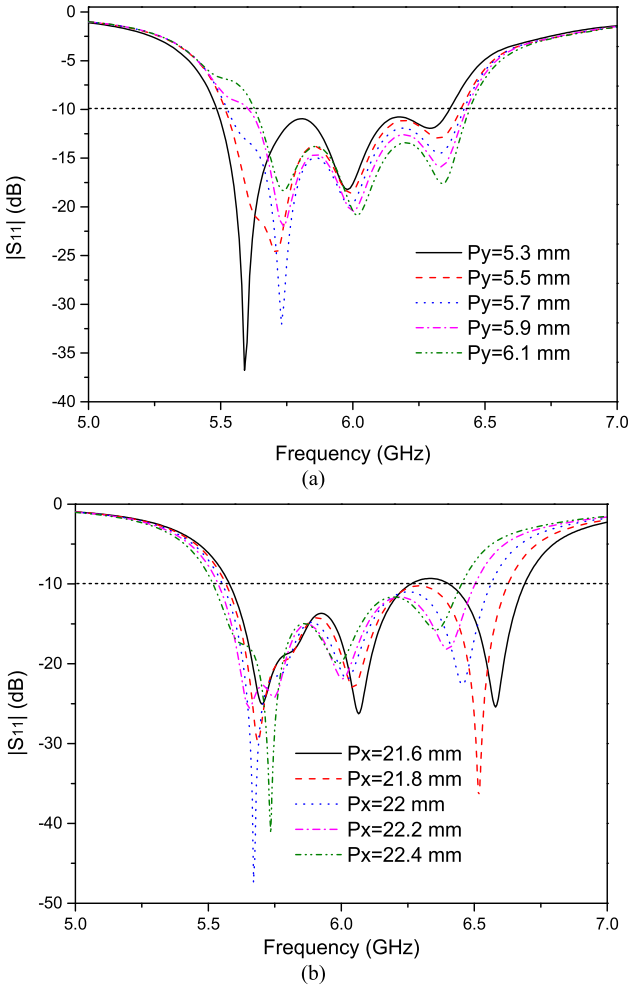

FIGURE 11. Simulated frequency responses of the antenna ANT_4 against (a) Py, where $L_1 = 13.1$ mm, $L_2 = 13.5$ mm, $L_5 = 5.35$ mm, $\theta = 47°$, $w_1 = 1.2$ mm, $w_2 = 0.6$ mm, $r = 0.65$ mm, $s = 0.8$ mm, $Px = 22.6$ mm, and (b) Px, where $L_1 = 13.1$ mm, $L_2 = 13.5$ mm, $L_5 = 5.35$ mm, $\theta = 47°$, $w_1 = 1.2$ mm, $w_2 = 0.6$ mm, $r = 0.65$ mm, $s = 0.8$ mm, Py=5.7 mm.

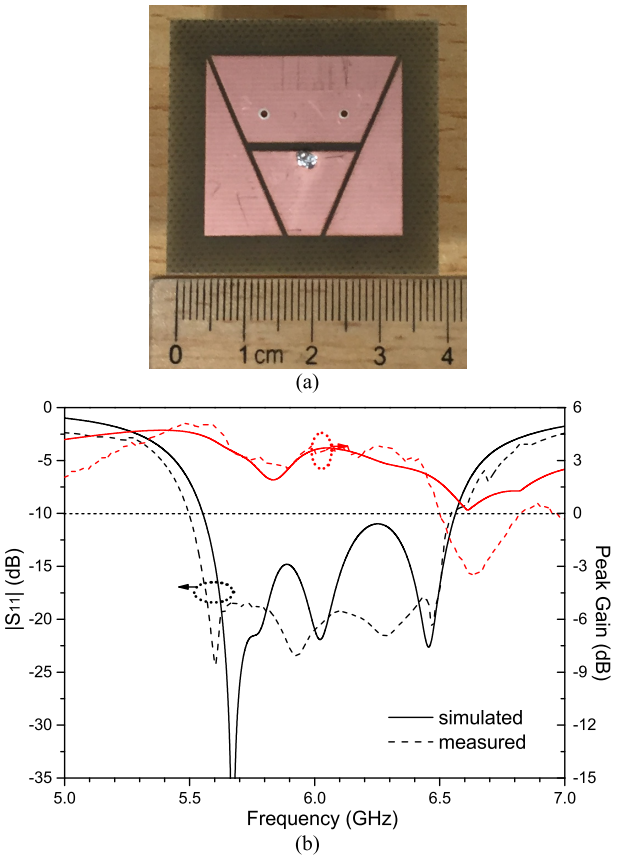

FIGURE 12. (a) Photograph and (b) simulated and measured reflection coefficients and peak gains of the proposed antenna ANT_4.

connector from the back of the substrate. The photograph of the fabricated antenna is shown in Fig. 8(a).

The simulated and measured reflection coefficients, peak gains, and radiation patterns of the proposed antenna ANT_3' are illustrated in Fig. 8(b) and Fig. 9, respectively. The measured impedance bandwidth with $|S_{11}| < -10$ dB is from 5.46 to 6.27 GHz (13.8%) as shown in Fig. 8(b). Besides, there are three resonances at 5.7 GHz, 5.97 GHz and 6.2 GHz, respectively. For radiation characteristics, the simulated and measured realized peak gains versus operating frequencies are also given, where the measurements are basically in agreement with the simulated results. Fig. 9 plots the simulated and measured radiation patterns in E-plane (xz-plane) and H-plane (yz-plane) at 5.7 GHz, 6.0 GHz and 6.2 GHz, respectively. It indicates that the proposed antenna has realized good far-field characteristics both in the E-plane and H-plane within the frequency band. The differences between simulated and measured results are attributed to the soldering of the SMA connector and measuring environment.

III. DESIGN OF THE PROPOSED PATCH ANTENNA WITH BOTH OF MULTIPLE PARASITIC PATCHES AND SHORTING VIAS

Based on the microstrip patch antenna ANT_3', two shorting vias are employed to construct the antenna ANT_4 in order to further enhance the impedance bandwidth as shown in Fig. 10(a). As analyzed in Fig. 3(b), the surface current distribution of the TM_{12} mode has two periods of variation on the trapezoidal patch P1. When the shorting vias are inserted into the position where the surface current is concentrated, the change of current distribution on the antenna patch will occur, thus the input impedance of the antenna at some frequency ranges will be reduced toward 50 Ohm, resulting in the increase of the impedance bandwidth. Comparisons between the antennas with and without shorting vias are shown in Fig. 10(b) and (c), where the parameters of the antenna ANT_4 are optimized on the basis of the antenna ANT_3'. In Fig. 10(b), the input resistance and reactance of the antenna with shorting vias (ANT_4) are more stable than those of the antenna without shorting vias (ANT_3'), which indicates that the shorting vias have significant effect on the improvement of the impedance bandwidth. Fig. 10(c) illustrates the bandwidth comparisons of these two antennas. The simulated impedance bandwidth with $|S_{11}| < -10$ dB of the antenna ANT_3' is from 5.56 to 6.28 GHz while the

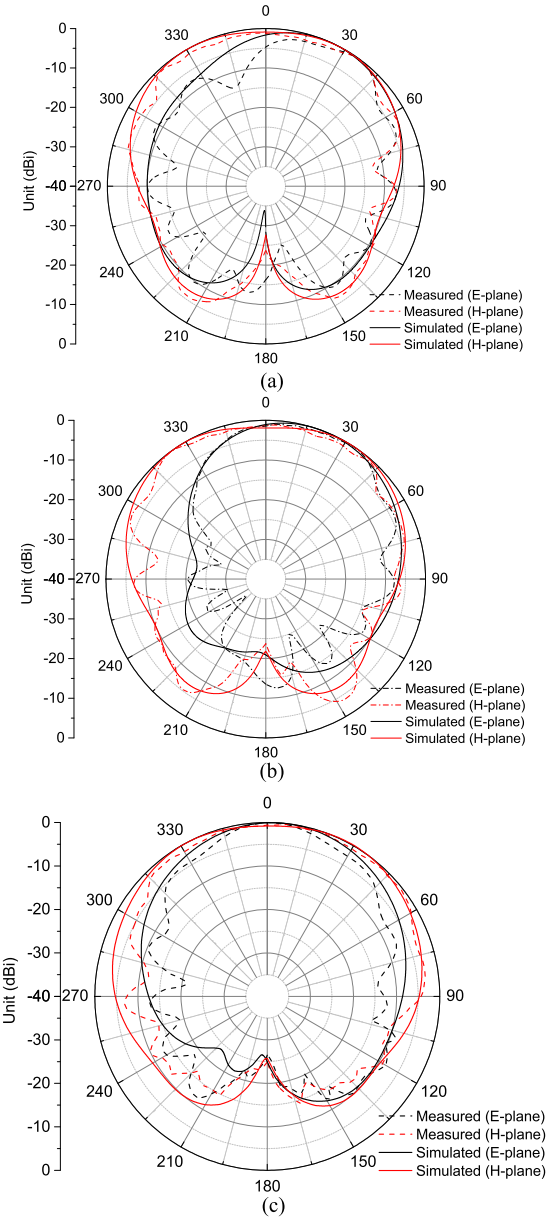

FIGURE 13. Simulated and measured radiation patterns at (a) 5.7 GHz, (b) 6 GHz and (c) 6.3 GHz.

bandwidth of its counterpart antenna ANT_4 is from 5.47 to 6.38 GHz. Obviously, the latter one has been enhanced owing to the added shorting vias.

Some parametric studies on the placement of the shorting vias have been done for the bandwidth optimization as shown in Fig. 11. The key parameters P_x and P_y, i.e., the positions of the shorting vias, should be appropriately adjusted to satisfy the required impedance bandwidth of the antenna. Finally, a microstrip patch antenna with both of multiple parasitic patches two shorting vias is designed and measured, whose fabricated photograph is shown in Fig. 12(a). The dimensions of the antenna are chosen as $L = 36$ mm, $W = 39$ mm, $L_1 = 18.8$ mm, $L_2 = 13.5$ mm, $L_5 = 5.4$ mm, $w_1 = 1.2$ mm, $w_2 = 0.6$ mm, $s = 0.8$ mm, $\theta = 47°$, $P_y = 5.7$ mm, $P_x = 22$ mm, and the radii of the probe and shorting vias are $r = 0.65$ mm and $R_v = 0.5$ mm, respectively.

Fig. 12(b) and Fig. 13 show the simulated and measured reflection coefficients, peak gain and radiation patterns of the designed antenna with both of the parasitic patches and shorting vias, respectively. As shown in Fig. 12(b), the simulated impedance bandwidth with $|S_{11}| < -10$ dB is from 5.56 to 6.55 GHz (16.5%) while the measured counterpart is from 5.5 to 6.55 GHz (17.4%). Meanwhile, the simulated and measured peak gains of the antenna versus frequencies are also shown. Fig. 13 plots the simulated and measured radiation patterns of the antenna ANT_4 in E-plane and H-plane at 5.7, 6.0 and 6.3 GHz, respectively, which are similar to the radiation pattern results of the antenna ANT_3' shown in Fig. 9.

IV. CONCLUSION

In this paper, a novel microstrip patch antenna with multiple parasitic patches for three resonances generation has been designed firstly. When the parasitic patches are introduced in the structure of the proposed antenna, two extra resonances can be obtained, thus the bandwidth will be broadened effectively. Parametric study has been explored to analyze the effects of dimensional parameters on the performance of the antenna. Then, two shorting vias are added based on the above proposed antenna, consequently, the input impedance can be lowered at some frequency ranges and thus the bandwidth will be further broadened. To validate the design ideas, two examples of the proposed antennas have been fabricated and tested. The measured results of these two antennas show that the impedance bandwidths with $|S_{11}| < -10$ dB range from 5.46 to 6.27 GHz (13.8%) and 5.5 to 6.55 GHz (17.4%), respectively. Both of them can achieve good far-field radiation patterns within the operating frequency bands.

REFERENCES

[1] D. M. Pozar, "Microstrip antennas," *Proc. IEEE*, vol. 80, no. 1, pp. 79–91, Jan. 1992.
[2] K. F. Lee and K. M. Luk, *Microstrip Patch Antennas*. London, U.K.: Imperial College Press, 2011.
[3] J.-Y. Sze and K.-L. Wong, "Slotted rectangular microstrip antenna for bandwidth enhancement," *IEEE Trans. Antennas Propag.*, vol. 48, no. 8, pp. 1149–1152, Aug. 2000.
[4] J.-H. Lu, "Bandwidth enhancement design of single-layer slotted circular microstrip antennas," *IEEE Trans. Antennas Propag.*, vol. 51, no. 5, pp. 1126–1129, May 2003.
[5] A. A. Deshmukh, "Broadband slot cut shorted sectoral microstrip antennas," *IET Microw., Antennas Propag.*, vol. 11, no. 9, pp. 1280–1287, Jul. 2017.
[6] A. Kandwal and S. K. Khah, "A novel design of gap-coupled sectoral patch antenna," *IEEE Antennas Wireless Propag. Lett.*, vol. 12, pp. 674–677, 2013.
[7] Z. Liang, J. Liu, Y. Zhang, and Y. Long, "A novel microstrip quasi Yagi array antenna with annular sector directors," *IEEE Trans. Antennas Propag.*, vol. 63, no. 10, pp. 4524–4529, Oct. 2015.
[8] J. Wu, Y. Yin, Z. Wang, and R. Lian, "Broadband circularly polarized patch antenna with parasitic strips," *IEEE Antennas Wireless Propag. Lett.*, vol. 14, pp. 559–562, 2015.
[9] W. S. T. Rowe and R. B. Waterhouse, "Investigation into the performance of proximity coupled stacked patches," *IEEE Trans. Antennas Propag.*, vol. 54, no. 6, pp. 1693–1698, Jun. 2006.

[10] H. Wong, K. K. So, and X. Gao, "Bandwidth enhancement of a monopolar patch antenna with V-shaped slot for car-to-car and WLAN communications," *IEEE Trans. Veh. Technol.*, vol. 65, no. 3, pp. 1130–1136, Mar. 2016.
[11] J. Liu, Q. Xue, H. Wong, H. W. Lai, and Y. Long, "Design and analysis of a low-profile and broadband microstrip monopolar patch antenna," *IEEE Trans. Antennas Propag.*, vol. 61, no. 1, pp. 11–18, Jan. 2013.
[12] J. Liu and Q. Xue, "Broadband long rectangular patch antenna with high gain and vertical polarization," *IEEE Trans. Antennas Propag.*, vol. 61, no. 2, pp. 539–546, Feb. 2013.
[13] J. Wang, Q. Liu, and L. Zhu, "Bandwidth enhancement of a differential-fed equilateral triangular patch antenna via loading of shorting posts," *IEEE Trans. Antennas Propag.*, vol. 65, no. 1, pp. 36–43, Jan. 2017.
[14] T. L. Wu, Y. M. Pan, P. F. Hu, and S. Y. Zheng, "Design of a low profile and compact omnidirectional filtering patch antenna," *IEEE Access*, vol. 5, pp. 1083–1089, 2017.
[15] Y. Shi, J. Liu, and Y. Long, "Wideband triple- and quad-resonance substrate integrated waveguide cavity-backed slot antennas with shorting vias," *IEEE Trans. Antennas Propag.*, vol. 65, no. 11, pp. 5768–5775, Nov. 2017.
[16] ANSYS Corp. (2012). *ANSYS High Frequency Structure Simulator (HFSS), ver. 13.0*. [Online]. Available: http://www.ansoft.com
[17] K. P. Ray and G. Kumar, "Determination of the resonant frequency of microstrip antennas," *Microw. Opt. Technol. Lett.*, vol. 23, no. 2, pp. 114–117, 1999.

KAI DA XU (S'13–M'15) received the B.S. and Ph.D. degrees in electromagnetic field and microwave technology from the University of Electronic Science and Technology of China (UESTC), Chengdu, China, in 2009 and 2015, respectively.

From 2012 to 2014, he was a Visiting Researcher with the Department of Electrical and Computer Engineering, Duke University, Durham, NC, USA, under the financial support from the China Scholarship Council. From 2016 to 2017, he was a Post-Doctoral Fellow with the State Key Laboratory of Millimeter Waves, City University of Hong Kong, Hong Kong. He is currently an Assistant Professor with the Institute of Electromagnetics and Acoustics and also with the Department of Electronic Science, Xiamen University, Xiamen, China. He has authored or co-authored over 70 papers in peer-reviewed journals and conference proceedings. His current research interests include RF/microwave and millimeter-wave circuits, antenna arrays, and nanoscale memristors.

Dr. Xu received the UESTC Outstanding Graduate Award in 2009 and 2015, respectively. He received the National Graduate Student Scholarship from the Ministry of Education, China, in 2012, 2013, and 2014. He serves as a reviewer for several IEEE and IET journals, including the IEEE Transactions on Microwave Theory and Techniques, the IEEE Transactions on Electron Devices, the IEEE Transactions on Computer-Aided Design of Integrated Circuits and Systems, the IEEE Antennas and Wireless Propagation Letters, the IEEE Microwave and Wireless Components Letters, the IEEE Access, the *IET Microwaves Antennas and Propagation*, and the *Electronics Letters*. Since 2017, he has been serving as an Associate Editor for the IEEE Access and *Electronics Letters*. He is also an Editorial Board Member of the *AEÜ-International Journal of Electronics and Communications*.

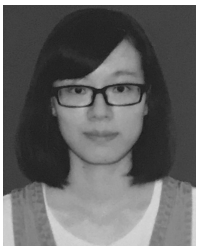

HAN XU was born in Quanzhou, Fujian, China, in 1992. She received the B.Eng. degree in electronic science and technology from the Nanjing University of Aeronautics and Astronautics, Nanjing, China, in 2015.

She is currently pursuing the M.Eng. degree with Xiamen University, Xiamen, China. Her current research interests include microstrip filters and antennas.

YANHUI LIU (M'15) received the B.S. and Ph.D. degrees in electrical engineering from the University of Electronic Science and Technology of China (UESTC), Sichuan, China, in 2004 and 2009, respectively.

From 2007 to 2009, he was a Visiting Scholar with the Department of Electrical Engineering, Duke University, Durham, NC, USA. Since 2011, he has been with Xiamen University, Xiamen, China, where he is currently a Full Professor with the Department of Electronic Science. From September to December in 2017, he was a Visiting Professor with the State Key Laboratory of Millimeter Waves in City University of Hong Kong. He has authored or co-authored over 100 peer-reviewed journal and conference papers. He holds several granted Chinese patents. His current research interests include antenna array design, array signal processing, and microwave imaging methods.

Dr. Liu is a Senior Member of the Chinese Institute of Electronics (CIE), a Committee Member of the CIE Antenna Society and its Electromagnetic Scattering and Inverse Scattering Branch. He received the UESTC Outstanding Graduate Award in 2004 and the Excellent Doctoral Dissertation Award of Sichuan Province of China in 2012. He is currently serving as an Associate Editor for the IEEE Access and a Reviewer for several international journals, including the IEEE Transactions on Antennas and Propagation, IEEE Transactions on Geosciences and Remote Sensing, IEEE Antennas and Wireless Propagation Letters, IEEE Microwave and Wireless Components Letters, *IET Microwave, Antennas and Propagation*, and *Digital Signal Processing*.

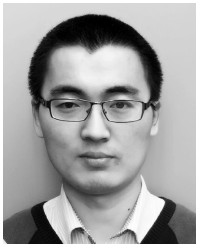

JIANXING LI received the B.S., M.S., and Ph.D. degrees in electromagnetic field and microwave technology from Xi'an Jiaotong University, Xi'an, China, in 2008, 2011, and 2016, respectively.

From 2014 to 2016, he was a Visiting Researcher with the Department of Electrical and Computer Engineering, Duke University, Durham, NC, USA, under the financial support from the China Scholarship Council. He is currently a Lecturer with the School of Electronic and Information Engineering, Xi'an Jiaotong University. His current research interests include microwave circuits, antennas, and metamaterials.

QING HUO LIU (S'88–M'89–SM'94–F'05) received the B.S. and M.S. degrees in physics from Xiamen University, China, and the Ph.D. degree in electrical engineering from the University of Illinois, Urbana–Champaign, IL, USA.

He was a Research Assistant with the Electromagnetics Laboratory, University of Illinois at Urbana–Champaign, from 1986 to 1988, where he was a Post-Doctoral Research Associate from 1989 to 1990. He was a Research Scientist and the Program Leader with Schlumberger-Doll Research, Ridgefield, CT, USA, from 1990 to 1995. From 1996 to 1999, he was an Associate Professor with New Mexico State University. Since 1999, he has been with Duke University, where he is currently a Professor of electrical and computer engineering. He has authored over 400 papers in refereed journals and 500 papers in conference proceedings. His research interests include computational electromagnetics and acoustics, inverse problems, and their application in nanophotonics, geophysics, biomedical imaging, and electronic packaging.

Dr. Liu received the 1996 Presidential Early Career Award for Scientists and Engineers from the White House, the 1996 Early Career Research Award from the Environmental Protection Agency, and the 1997 CAREER Award from the National Science Foundation. He received the ACES Technical Achievement Award in 2017. He served as a Distinguished Lecturer for the IEEE Antennas and Propagation Society from 2014 to 2016. He is a Fellow of the Acoustical Society of America, the Electromagnetics Academy, and the Optical Society of America. He currently serves as the founding Editor-in-Chief of the new IEEE JOURNAL ON MULTISCALE AND MULTIPHYSICS COMPUTATIONAL TECHNIQUES, the Deputy Editor-in-Chief of *Progress in Electromagnetics Research*, and an Editor of the *Journal of Computational Acoustics*.